

The fate of a single impurity in the Bose-Hubbard model

Chao Zhang^{1,*}

¹*Department of Physics, Anhui Normal University, Wuhu, China*

We map out the global phase diagram of a single mobile impurity in the two-dimensional Bose-Hubbard model, spanning the bath evolution from a compressible superfluid (SF) to an incompressible Mott insulator (MI) and the full range of impurity-bath coupling. Using sign-problem-free worm-algorithm quantum Monte Carlo method, we identify two sharply distinct localization mechanisms that organize the entire diagram. In the compressible SF, increasing impurity-bath coupling $|U_{ib}|$ drives an *interaction-driven winding-collapse crossover*: a light, extended polaron with finite winding evolves continuously into a heavy polaron and ultimately a self-trapped state—a repulsive *saturated bubble* or an attractive *bound cluster*—even while the bath remains globally superfluid, establishing localization without any bath phase transition. By contrast, upon tuning the bath across the SF-MI transition at fixed impurity-bath coupling U_{ib} , localization becomes *compressibility controlled*: the vanishing bath compressibility quenches polaronic dressing and collapses the impurity-centered density response, converting the polaron into an almost free defect and, deep in the MI, into a fully localized vacancy or particle defect. In the incompressible regime, localization proceeds via *quantized defect formation*, manifested by discrete changes in the total bath occupation. Together, our results provide a unified microscopic picture of impurity localization in correlated lattice bosons, governed by winding collapse in the SF and compressibility-driven localization across the SF-MI transition.

Introduction— A single mobile impurity embedded in a quantum many-body medium provides a minimal yet stringent probe of correlations, coherence, and transport. In weakly interacting Bose gases, the impurity forms a well-defined Bose polaron: a coherent quasiparticle with finite residue, a renormalized effective mass, and an extended dressing cloud built from gapless density fluctuations[1–9]. A central question is how this quasiparticle picture ultimately breaks down as correlations grow. In particular, can an impurity lose mobility and localize *purely through interactions* even in an otherwise uniform, translation-invariant superfluid, and how does this fate change when the bath itself becomes incompressible?

The two-dimensional Bose-Hubbard model at *unit filling* ($\langle n_b \rangle = 1$) offers an ideal setting to address these questions [10–13]. By tuning the intra-bath interaction U_b/t , the bath evolves from a compressible superfluid (SF) to an incompressible Mott insulator (MI). Adding a single impurity with local impurity-bath coupling U_{ib} (repulsive or attractive) poses a sharply defined fate problem: *what are the distinct regimes of impurity motion and localization across the full $(U_b/t, U_{ib}/t)$ parameter space, and what microscopic mechanisms separate them?*

While the limiting regimes are qualitatively understood [14–20], their global connection remains incomplete. In a compressible SF, most studies emphasize the coherent and delocalized polaron regime, where the impurity remains mobile and its dressing is supported by long-wavelength density fluctuations. In a deep MI, the bath has a gap and vanishing compressibility; weak coupling tends to leave the impurity as an almost free defect with minimal dressing, whereas strong coupling can bind the impurity to localized vacancy- or particle-defect. However, a unified picture of *how* impurity transport and dressing are lost—either by increasing $|U_{ib}|$ in the SF or by quenching bath compressibility across the SF-MI transition—has not been established. In particular, interaction-driven winding-collapse localization without

any bath phase transition in a uniform SF background has remained an open issue.

Here we resolve this problem by constructing the *global phase diagram* of a single mobile impurity in the two-dimensional Bose-Hubbard model at $\langle n_b \rangle = 1$. We employ large-scale, sign-problem-free worm-algorithm quantum Monte Carlo [21–24] to obtain unbiased equilibrium results across both SF and MI regimes. Crucially, we go beyond characterizing the impurity alone and track the *microscopic bath response*—the impurity-induced density redistribution and its collapse as the bath loses compressibility. Our diagnostics include impurity transport from winding statistics, impurity coherence from single-particle correlations, and the bath response from impurity-centered density modulations; in the MI, we further identify *quantized* vacancy/interstitial defects through discrete changes in the total bath occupation.

The resulting phase diagram is organized by two sharply distinct localization mechanisms. *Within the compressible SF*, increasing $|U_{ib}|$ drives an *interaction-driven winding-collapse crossover*: a light, extended polaron with finite winding evolves continuously into a heavy polaron and ultimately self-traps into a compact bound state—a repulsive *saturated bubble* or an attractive *bound cluster*—even while the bath remains globally superfluid. This establishes localization without any bath phase transition, controlled by the impurity-bath interaction through a loss of winding transport. *Across the SF-MI transition at fixed U_{ib}* , localization becomes *compressibility controlled*: as bath compressibility is quenched, polaronic dressing and the impurity-induced density response collapse, and deep in the MI the impurity locks into a pinned vacancy (repulsive) or particle (attractive) defect with a *quantized ± 1* change in the total bath occupation. Together, these results provide a unified microscopic framework for impurity localization in correlated lattice bosons, governed by winding collapse in the SF and compressibility-driven localization across the SF-MI transition.

Model and observables— We consider the two-dimensional Bose–Hubbard model with a single distinguishable mobile impurity coupled to a bosonic bath,

$$H = -t_{\text{imp}} \sum_{\langle i,j \rangle} (a_i^\dagger a_j + \text{H.c.}) + U_{\text{ib}} \sum_i n_{\text{imp},i} n_{\text{b},i} \\ - t_{\text{b}} \sum_{\langle i,j \rangle} (b_i^\dagger b_j + \text{H.c.}) + \frac{U_{\text{b}}}{2} \sum_i n_{\text{b},i} (n_{\text{b},i} - 1) \\ - \mu_{\text{b}} \sum_i n_{\text{b},i}, \quad (1)$$

Here b_i (a_i) annihilates a bath (impurity) boson on site i , $n_{\text{b},i} = b_i^\dagger b_i$ and $n_{\text{imp},i} = a_i^\dagger a_i$ are the corresponding number operators, and t_{b} (t_{imp}) denotes the nearest-neighbor hopping amplitude of the bath (impurity). We restrict to the single-impurity limit $\sum_i n_{\text{imp},i} = 1$, and the filling $\langle n_{\text{b},i} \rangle = 1$ for the bath. The on-site interaction U_{b} tunes the bath from a compressible superfluid (SF) to an incompressible Mott insulator (MI), while the impurity–bath coupling U_{ib} can be either repulsive ($U_{\text{ib}} > 0$) or attractive ($U_{\text{ib}} < 0$).

We set $t_{\text{b}} = t_{\text{imp}} = t = 1$ as the energy unit and vary U_{b}/t from 8.0 (deep SF) to 24.0 (deep MI). All simulations are performed on $L \times L$ lattices (typically $L = 20$) at inverse temperature $\beta = L$ with periodic boundary condition, which ensures convergence to the ground-state regime.

Polaron properties— We access impurity quasiparticle properties via the single-impurity Green’s function measured within the worm algorithm. We accumulate the real-space impurity Green’s function $G_{\text{imp}}(\mathbf{r}, \tau) = \langle a(\mathbf{r}, \tau) a^\dagger(\mathbf{0}, 0) \rangle$ and obtain the momentum-resolved Green’s function by a discrete Fourier transform, $G_{\text{imp}}(\mathbf{k}, \tau) = \sum_{\mathbf{r}} e^{-i\mathbf{k} \cdot \mathbf{r}} G_{\text{imp}}(\mathbf{r}, \tau)$. At low temperature and large imaginary time, $G_{\text{imp}}(\mathbf{k}, \tau)$ is dominated by the lowest impurity state, $G_{\text{imp}}(\mathbf{k}, \tau) \simeq Z_{\mathbf{k}} e^{-E_p(\mathbf{k})\tau}$, from which we extract the polaron energy $E_p(\mathbf{k})$ and quasiparticle residue $Z_{\mathbf{k}}$. The effective mass $m^*/m_0 = 2t/\frac{\partial^2 E_p(\mathbf{k})}{\partial \mathbf{k}^2}$ is obtained from the small-momentum dispersion by fitting the lowest available momenta.

Winding-number diagnostics— To characterize impurity mobility and the global coherence of the bath, we measure the winding numbers of both components. For the impurity, we record the winding number square of the impurity $\langle W_{\text{imp}}^2 \rangle = \langle W_{\text{imp},x}^2 + W_{\text{imp},y}^2 \rangle$, where $W_{\text{imp},x}$ and $W_{\text{imp},y}$ denote the net worldline crossings through the x and y directions. A finite $\langle W_{\text{imp}}^2 \rangle$ signals a mobile impurity with extended trajectories, while $\langle W_{\text{imp}}^2 \rangle \rightarrow 0$ indicates complete localization. For the bath, the corresponding estimator gives the superfluid density $\rho_s^{\text{bath}} = \langle W_{\text{bath},x}^2 + W_{\text{bath},y}^2 \rangle / (2t_b \beta)$, directly related to the superfluid density via the Pollock–Ceperley relation [25].

Bath response diagnostics— To quantify the spatial response of the bath to a single impurity, we evaluate the impurity-centered correlator $C_{\text{ib}}(\mathbf{r}) = \sum_{\mathbf{r}_{\text{imp}}} w(\mathbf{r}_{\text{imp}}) [\langle n_{\text{b}}(\mathbf{r}_{\text{imp}} + \mathbf{r}) \rangle - \bar{n}_{\text{b}}]$, which measures the bath density change at displacement \mathbf{r} from the instantaneous impurity position \mathbf{r}_{imp} . Here $\bar{n}_{\text{b}} = L^{-2} \sum_i \langle n_{\text{b},i} \rangle$ is the uniform bath density. Because the impurity is a quantum object whose worldline freely ex-

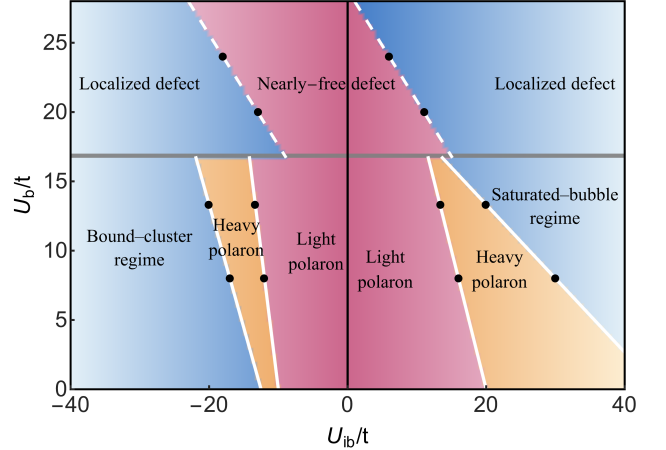


FIG. 1. **Phase diagram of a single impurity in the two-dimensional Bose–Hubbard model in the $(U_{\text{ib}}/t, U_{\text{b}}/t)$ plane.** The vertical dashed line separates repulsive ($U_{\text{ib}}/t > 0$) and attractive ($U_{\text{ib}}/t < 0$) impurity–bath couplings, while the horizontal dashed line marks the superfluid–Mott transition of the bath ($U_{\text{b}}/t \simeq 16.7$). In the *compressible superfluid* region ($U_{\text{b}}/t < 16.7$), increasing $|U_{\text{ib}}|/t$ drives an *interaction-driven, winding-collapse polaron localization*: a mobile light polaron continuously evolves into a heavy polaron and, for sufficiently strong coupling, into a saturated bubble (repulsive side) or a bound cluster (attractive side). In the *incompressible Mott-insulating* regime ($U_{\text{b}}/t \gtrsim 16.7$), the impurity localizes by *quantized defect formation*. Upon increasing $|U_{\text{ib}}|/t$ beyond a threshold, the impurity changes abruptly from a nearly free defect to a pinned vacancy (repulsive) or particle (attractive) defect, signaled by an integer-valued bath occupation change. For intermediate couplings, the impurity remains only weakly dressed and essentially free. Along vertical cuts at fixed U_{ib}/t , crossing the SF–MI boundary thus realizes *compressibility-controlled localization*. Black dots mark QMC data points; solid white lines are guides to the eye highlighting continuous crossover boundaries in the superfluid, while dotted lines indicate sharp transitions between distinct defect regimes in the Mott phase.

plores the lattice in imaginary time, its position is not fixed. The weighting function $w(\mathbf{r}_{\text{imp}}) = \beta^{-1} \int_0^\beta \langle n_{\text{imp}}(\mathbf{r}_{\text{imp}}, \tau) \rangle d\tau$ represents the time-averaged probability of finding the impurity at site \mathbf{r}_{imp} , satisfying $\sum_{\mathbf{r}_{\text{imp}}} w(\mathbf{r}_{\text{imp}}) = 1$.

To remove lattice anisotropy, we perform a rotational averaging over all lattice sites with the same Euclidean distance $R = |\mathbf{r}| = \sqrt{r_x^2 + r_y^2}$ (using the minimum-image convention), defining $C_{\text{ib}}(R) = N_R^{-1} \sum_{|\mathbf{r}|=R} C_{\text{ib}}(\mathbf{r})$, where N_R counts sites satisfying $|\mathbf{r}| = R$. This smooth radial profile characterizes the impurity-centered bath density deformation: $C_{\text{ib}}(R) < 0$ signals a local depletion (*bubble*) for repulsive $U_{\text{ib}}/t > 0$, while $C_{\text{ib}}(R) > 0$ indicates a density accumulation (*cluster*) for attractive $U_{\text{ib}}/t < 0$. The cumulative excess $\Delta N(R) = \sum_{|\mathbf{r}| \leq R} C_{\text{ib}}(\mathbf{r})$ gives the net bath particle-number change within a disk of radius R centered at the impurity, whose amplitude and extent distinguish the light, heavy, and localized regimes discussed below.

Together, these observations reveal a clear dichotomy in

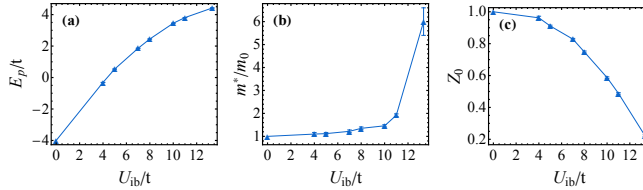


FIG. 2. **Impurity quasiparticle properties in a superfluid bath** ($U_b/t = 13.3$). (a) Ground-state energy E_p/t , (b) effective mass m^*/m_0 (with $m_0 = 1/2t = 1/2$ the bare particle mass), and (c) quasiparticle residue Z_0 as functions of repulsive impurity-bath coupling U_{ib}/t . All data correspond to finite impurity winding $\langle W_{\text{imp}}^2 \rangle > 0$, where a mobile light polaron is well defined. Increasing U_{ib} continuously enhances mass renormalization and suppresses Z_0 , reflecting stronger impurity–bath correlations. Beyond $U_{ib}/t \gtrsim 13.3$, the winding number vanishes (shown in Figure 3(e)), and the quasiparticle description breaks down, marking the boundary of the light-polaron regime. The ground-state energy changes smoothly throughout, confirming a continuous interaction-driven crossover rather than a sharp transition.

how impurity localizes in correlated Bose-Hubbard model, as shown in Fig. 1. In the compressible superfluid bath ($U_b/t \lesssim 16.7$), localization is a continuous process: increasing $|U_{ib}|/t$ gradually suppresses coherent winding and compresses the dressing cloud, producing the smooth crossover from light polarons to heavy polarons and ultimately to saturated-bubble (repulsive) or bound-cluster (attractive) states. We refer to this mechanism as *interaction-driven winding-collapse polaron localization*.

In contrast, when impurity-bath coupling U_{ib}/t is held fixed and bath interaction U_b/t is increased across the SF–MI transition, the bath compressibility—not impurity-bath coupling strength—controls localization. Polaronic dressing collapses abruptly upon entering the incompressible regime, and the impurity instead undergoes an abrupt transition from a mobile nearly-free defect to a pinned localized defect carrying an integer excess (+1) or deficit (−1) of bath occupation. We refer to this as the *compressibility-controlled localization* mechanism.

These two localization routes—continuous, interaction-driven winding-collapse in a superfluid bath and compressibility-controlled localization across the SF–MI transition, which at strong bath interaction (deep MI regime) culminates in quantized defect formation—constitute two fundamentally distinct paradigms of impurity physics in strongly correlated bosonic matter.

Interaction-driven polaron localization in a superfluid bath: (i) *Quasiparticle renormalization in the light-polaron regime.* To characterize the impurity in a compressible superfluid background, we fix the bath interaction at $U_b/t = 13.3$ (deep in the SF phase) and increase the repulsive impurity-bath coupling $U_{ib}/t > 0$. Figure 2 shows the ground-state energy E_p/t , effective mass m^*/m_0 with $m_0 = 1/2t = 1/2$ the bare particle mass, and quasiparticle residue Z_0 extracted from imaginary-time Green’s functions, restricted to the regime with finite winding $\langle W_{\text{imp}}^2 \rangle > 0$, where a mobile

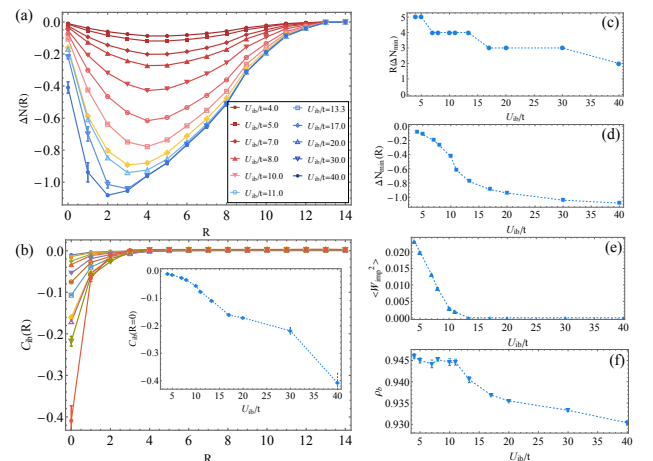


FIG. 3. **Real-space crossover from a light polaron to a saturated bubble in the superfluid bath** ($U_b/t = 13.3$). (a) Cumulative bath-density response $\Delta N(R)$ for increasing impurity–bath coupling U_{ib}/t . Red curves denote the light-polaron regime, the single orange curve highlights the heavy-polaron regime, and blue curves correspond to the saturated-bubble regime where the impurity becomes localized. (b) Impurity–centered correlation $C_{ib}(R)$ and its on-site contrast $C_{ib}(0)$ (inset). (c,d) Position R_{\min} and depth ΔN_{\min} of the depletion minimum extracted from $\Delta N(R)$. (e) Impurity winding number $\langle W_{\text{imp}}^2 \rangle$, exhibiting the continuous loss of coherent motion. (f) Bath superfluid density ρ_b , which remains nearly constant across the crossover. The color evolution illustrates the continuous crossover from a mobile light polaron (red) to a compact heavy polaron (orange), and finally to a fully localized saturated bubble (blue).

polaron is well defined.

At weak impurity-bath coupling ($U_{ib}/t \lesssim 10.0$), the impurity forms a light polaron: $m^*/m_0 \lesssim 2.0$, $Z_0 \gtrsim 0.5$, and the energy varies smoothly, indicating negligible dressing. For intermediate coupling ($10.0 \lesssim U_{ib}/t \lesssim 13.3$), m^*/m_0 increases while Z_0 decreases continuously, reflecting enhanced impurity–bath correlations and increasing mass renormalization, yet coherent transport persists. Beyond this range ($U_{ib}/t \gtrsim 13.3$), the impurity winding number vanishes (shown in Fig. 3(e)), signaling the loss of coherent motion and the breakdown of the quasiparticle picture. Consequently, quantities such as m^*/m_0 increases abruptly and Z_0 decreases to zero, marking the boundary of the light-polaron to heavy-polaron regime. Throughout the mobile region, E_p/t evolves smoothly with U_{ib}/t , confirming that the dressing process is a smooth crossover rather than a sharp transition.

(ii) *Real-space crossover from light polaron to heavy polaron and saturated bubble state.* To elucidate how the impurity reshapes its surrounding superfluid environment, we fix the bath interaction at $U_b/t = 13.3$ (deep in the SF regime) and gradually increase the repulsive impurity–bath coupling $U_{ib}/t > 0$. Figure 3 summarizes the corresponding observables, revealing a continuous evolution from a mobile *light polaron* (red) to a *heavy polaron* (orange), and finally to a spatially *saturated-bubble state* (blue).

Figure 3(a) shows the cumulative bath-density response $\Delta N(R)$ for different impurity-bath coupling U_{ib} . At weak coupling ($U_{\text{ib}}/t < 13.3$), $\Delta N(R)$ exhibits a shallow, broad minimum around $R_{\text{min}} \approx 4\text{--}5$ with $\Delta N_{\text{min}} \lesssim -0.4$, indicating an extended depletion cloud, characteristic of a mobile light polaron. As U_{ib}/t increases to $13.3 \lesssim U_{\text{ib}}/t \lesssim 20.0$, the depletion deepens and contracts to $R_{\text{min}} \approx 2\text{--}3$, while ΔN_{min} approaches -0.8 . However, the impurity winding number has already dropped close to zero, indicating that although the cloud remains spatially extended, coherent motion is lost. This intermediate regime corresponds to a *heavy polaron*: localized in real space but still surrounded by a finite-size many-body dressing cloud. For $U_{\text{ib}}/t > 20$, all $\Delta N(R)$ traces collapse onto a universal profile beyond $R \simeq 4$, with the depth approaching but not exactly reaching -1 . This spatial convergence marks the onset of a *saturated-bubble state*: the depletion cloud has reached a fixed spatial extent and cannot shrink further, although its depth continues to increase with U_{ib}/t . This saturation is spatial, not quantized—unlike the integer defects encountered in the incompressible Mott background, see the details in [26].

Figure 3(b) shows the corresponding impurity-centered correlator $C_{\text{ib}}(R)$, whose rapid on-site suppression (inset) tracks the same crossover. For $U_{\text{ib}}/t > 20$, $C_{\text{ib}}(R > 1)$ becomes nearly coupling-independent, confirming that the dressing cloud has reached its saturated spatial extent. Figure 3(c–f) quantify this continuum crossover. The extracted R_{min} and ΔN_{min} clearly demonstrate the shrinking and deepening of the deformation cloud [Fig. 3(c,d)]. Meanwhile, the impurity winding estimator $\langle W_{\text{imp}}^2 \rangle$ [Fig. 3(e)] falls smoothly by nearly two orders of magnitude for $U_{\text{ib}}/t > 13.3$, signaling the loss of coherent worldline motion rather than a sharp phase transition from a light polaron to a heavy polaron. In contrast, the bath superfluid density ρ_b [f] remains finite and only weakly suppressed, confirming that the localization is interaction-driven while the bath superfluid stays globally coherent.

Collectively, these observables delineate three dressing regimes driven solely by U_{ib}/t : (i) a *light-polaron regime* (red), characterized by finite winding, a broad, weak depletion cloud extending over $R \gtrsim 4\text{--}5$, and coherent quasiparticle motion; (ii) a *heavy polaron regime* (yellow), where the winding number has already collapsed ($\langle W_{\text{imp}}^2 \rangle \approx 0$), yet $\Delta N(R)$ still displays a compact but finite-range deformation ($R \simeq 3\text{--}4$), signaling an immobile but still spatially dressed impurity; (iii) a *saturated-bubble regime* (blue), where all $\Delta N(R)$ curves beyond $R \simeq 2$ collapse onto a universal profile, indicating a fully localized defect with a *spatially saturated* depletion cloud. Unlike in the Mott background, this saturation is not quantized to -1 , but deepens continuously with increasing U_{ib}/t while the bath remains globally superfluid. This progression from mobile light polarons to spatially saturated bubble represents a continuous, non-singular localization route driven purely by impurity-bath coupling strength inside a compressible superfluid bath.

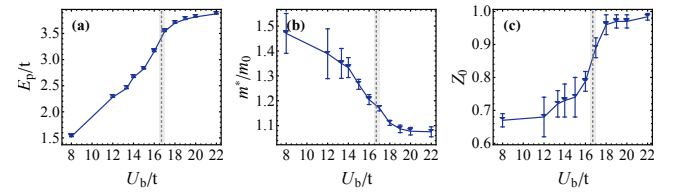


FIG. 4. **Compressibility-controlled collapse of polaronic dressing at a fixed repulsive impurity bath coupling $U_{\text{ib}}/t = 8.0$.** (a) Ground-state energy E_p/t , (b) effective-mass ratio m^*/m_0 , and (c) quasiparticle residue Z_0 as functions of bath interaction U_b/t . The shaded region marks the superfluid–MI transition of the bath ($U_b/t \simeq 16.7$). In the compressible superfluid regime ($U_b/t < 16.7$), the impurity exhibits a weakly renormalized light-polaron behavior with finite dressing cloud. As the bath becomes increasingly less compressible, m^*/m_0 decreases while Z_0 rises, indicating a collapse of polaronic dressing. Once the bath enters the incompressible MI regime ($U_b/t \gtrsim 16.7$), m^*/m_0 approaches unity and $Z_0 \rightarrow 1$, confirming the emergence of a nearly-free.

Compressibility-controlled collapse of polaronic dressing

(i) *Polaron renormalization under decreasing bath compressibility.* To isolate the role of the bath, we fix the impurity-bath coupling at a moderate repulsive value ($U_{\text{ib}}/t = 8.0$) and vary U_b/t across the superfluid–MI transition. Figures 4(a–c) show that in the compressible superfluid regime ($U_b/t < 16.7$), the impurity remains a well-defined polaron with finite winding [Fig. 5(e)]. As the bath becomes less compressible, the many-body dressing weakens: the effective mass m^*/m_0 decreases from ~ 1.5 toward 1.2 while the quasiparticle residue Z_0 increases from ~ 0.7 to nearly 0.9 . This trend reflects the fact that a less compressible bath is less able to mediate dressing, leading to a progressively *lighter* polaron, in contrast to the usual impurity-bath interaction-driven mass enhancement for a fixed bath interaction. Upon approaching the SF–MI boundary ($U_b/t \simeq 16.7$), E_p/t exhibits a visible change in slope, while $m^*/m_0 \rightarrow 1$ and $Z_0 \rightarrow 1$, signaling the collapse of many-body dressing and the recovery of an almost free impurity. Once the bath enters the incompressible Mott regime ($U_b/t \gtrsim 16.7$), extended density redistribution is prohibited, and the impurity can no longer sustain polaronic correlations. It reduces to a nearly free defect—a trivial particle with no spatial dressing and no quasiparticle renormalization.

This compressibility-controlled breakdown of polaronic dressing is fundamentally different from the interaction-driven self-trapping observed at large U_{ib}/t in the superfluid regime: here, localization does not originate from strong coupling, but from the inability of the bath to support collective screening.

(ii) *Real-space collapse and defect formation.* Figures 5(a,b) reveal how the real-space bath responses evolve under the same protocol. In the superfluid phase, $\Delta N(R)$ and $C_{\text{ib}}(R)$ exhibit an extended depletion cloud characteristic of a coherent polaron. As the bath becomes less compressible, both the depth $\Delta N_{\text{min}}(R)$ and spatial extent of the depletion $R(\Delta N_{\text{min}})$ shrink continuously, as quantified in Figs. 5(c,d).

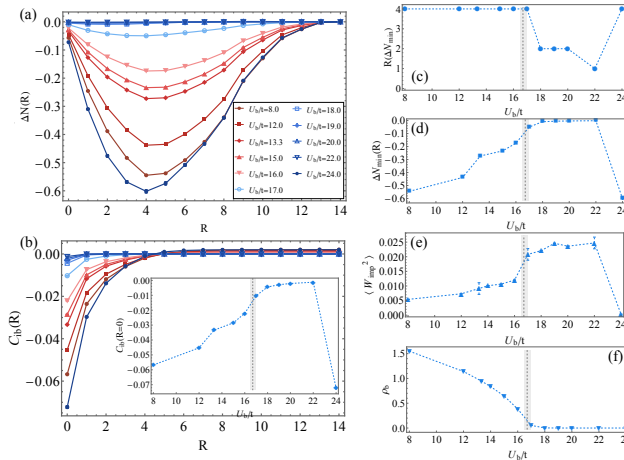


FIG. 5. **Compressibility-controlled collapse of polaronic dressing at fixed repulsive impurity bath coupling $U_{ib}/t = 8.0$.** (a) Cumulative bath-density depletion $\Delta N(R)$ and (b) impurity-centered correlator $C_{ib}(R)$ for increasing bath interaction U_b/t , color-coded from deep superfluid (dark red: $U_b/t = 8.0$) through intermediate (light red/orange: $U_b/t = 13.3, 15.0$) to near the transition (light blue: $U_b/t = 17.0$) and deep Mott regime (dark blue: $U_b/t = 20.0, 22.0, 24.0$). (c,d) Peak position $R(\Delta N_{\min})$ and depth $\Delta N_{\min}(R)$, showing the loss of extended bath correlations. (e) Impurity winding number $\langle W_{\text{imp}}^2 \rangle$ increases sharply once the bath loses compressibility, signaling the loss of coherent propagation. (f) Bath superfluid density ρ_b confirms that the collapse is driven by the vanishing bath compressibility. Together these observables reveal a compressibility-controlled crossover from a mobile polaron to a nearly free defect, and finally to a localized particle-defect in the MI background.

This collapse coincides with a sharp increase of the winding number (Fig. 5(e)), while the bath superfluid density vanishes (Fig. 5(f)), demonstrating that the breakdown is driven by the loss of compressibility. Inside the MI regime, the impurity first behaves as a nearly-free particle and then locks into a localized vacancy defect, characterized by quantized depletion $\Delta N(R) \rightarrow -1$. This represents the *compressibility-controlled localization* mechanism across the SF-MI transition, distinct from the continuous interaction-driven self-trapping in the superfluid.

MI extension and outlook— In an *incompressible* MI bath, extended density redistribution is forbidden and neither mobile polarons nor bound clusters survive. Increasing $|U_{ib}|/t$ then produces only short-range distortions, and quasiparticle signatures ($m^*/m_0, Z_0, \langle W_{\text{imp}}^2 \rangle$) revert toward their bare values. Deep in the Mott regime, strong coupling nucleates *quantized* particle or vacancy defects, signaled by a ± 1 change of the bath occupation; a systematic analysis of this insulating branch is reported in Ref. [26].

Several extensions are natural. Finite temperature should activate particle-hole excitations in the Mott background and induce a temperature-dependent delocalization crossover. Relaxing $t_a = t_b$ adds a powerful knob: $t_a \ll t_b$ approaches the static-defect limit, while $t_a \gg t_b$ realizes a fast impurity in a

slow correlated bath. Finally, the two-impurity sector can directly address bipolaron formation and transport by mapping binding energy and effective mass across the $(U_{ib}/t, U_b/t)$ plane, with an optional direct impurity-impurity coupling to separate bare from bath-mediated forces—all within the same sign-problem-free QMC framework. More discussion of experimental realizations and detection protocols is provided in our companion paper [26].

Acknowledgments— We are grateful to Guido Pupillo for bringing this idea to our attention and for helpful discussions. We thank Nikolay Prokof'ev for insightful discussions.

* chaozhang@ahnu.edu.cn

- [1] F. Grusdt, N. Mostaani, E. Demler, and L. A. P. Ardila, Impurities and polarons in bosonic quantum gases: a review on recent progress, *Reports on Progress in Physics* **88**, 066401 (2025).
- [2] F. Scazza, M. Zaccanti, P. Massignan, M. M. Parish, and J. Levinsen, Repulsive fermi and bose polarons in quantum gases, *Atoms* **10**, 10.3390/atoms10020055 (2022).
- [3] L. A. Peña Ardila and S. Giorgini, Impurity in a Bose-Einstein condensate: Study of the attractive and repulsive branch using quantum Monte Carlo methods, *Physical Review A* **92**, 033612 (2015).
- [4] L. A. Peña Ardila and S. Giorgini, Bose polaron problem: Effect of mass imbalance on binding energy, *Physical Review A* **94**, 063640 (2016).
- [5] L. A. Peña Ardila, N. B. Jørgensen, T. Pohl, S. Giorgini, G. M. Bruun, and J. J. Arlt, Analyzing the Bose polaron across resonant interactions, *Physical Review A* **99**, 063607 (2019).
- [6] L. A. Peña Ardila, G. M. Astrakharchik, and S. Giorgini, Strong-coupling Bose polarons in a two-dimensional gas, *Physical Review Research* **2**, 023405 (2020).
- [7] N.-E. Guenther, P. Massignan, M. Lewenstein, and G. M. Bruun, Bose polarons at finite temperature and strong coupling, *Phys. Rev. Lett.* **120**, 050405 (2018).
- [8] Y. Nakano, M. M. Parish, and J. Levinsen, Variational approach to the two-dimensional bose polaron, *Phys. Rev. A* **109**, 013325 (2024).
- [9] S. Van Loon, W. Casteels, and J. Tempere, Ground-state properties of interacting bose polarons, *Phys. Rev. A* **98**, 063631 (2018).
- [10] D. Jaksch, C. Bruder, J. I. Cirac, C. W. Gardiner, and P. Zoller, Cold bosonic atoms in optical lattices, *Phys. Rev. Lett.* **81**, 3108 (1998).
- [11] M. P. A. Fisher, P. B. Weichman, G. Grinstein, and D. S. Fisher, Boson localization and the superfluid-insulator transition, *Phys. Rev. B* **40**, 546 (1989).
- [12] B. Capogrosso-Sansone, N. V. Prokof'ev, and B. V. Svistunov, Phase diagram and thermodynamics of the three-dimensional bose-hubbard model, *Phys. Rev. B* **75**, 134302 (2007).
- [13] B. Capogrosso-Sansone, N. Prokof'ev, and B. Svistunov, Phase diagram and thermodynamics of the three-dimensional bose-hubbard model, *Phys. Rev. A* **77**, 015602 (2008).
- [14] R. Alhyder, V. E. Colussi, M. Čufar, J. Brand, A. Recati, and G. M. Bruun, Lattice Bose polarons at strong coupling and quantum criticality, *SciPost Phys.* **19**, 002 (2025).
- [15] M. Santiago-García, S. G. Castillo-López, and A. Camacho-Guardian, Lattice polaron in a bose-einstein condensate of hard-core bosons, *New Journal of Physics* **26**, 063015 (2024).

- [16] S. Dutta and E. J. Mueller, Variational study of polarons and bipolarons in a one-dimensional bose lattice gas in both the superfluid and the mott-insulator regimes, *Phys. Rev. A* **88**, 053601 (2013).
- [17] V. E. Colussi, F. Caleffi, C. Menotti, and A. Recati, Lattice polarons across the superfluid to mott insulator transition, *Phys. Rev. Lett.* **130**, 173002 (2023).
- [18] K. Keiler, S. I. Mistakidis, and P. Schmelcher, Doping a lattice-trapped bosonic species with impurities: from ground state properties to correlated tunneling dynamics, *New Journal of Physics* **22**, 083003 (2020).
- [19] S. Ding, G. A. Domínguez-Castro, A. Julku, A. Camacho-Guardian, and G. M. Bruun, Polarons and bipolarons in a two-dimensional square lattice, *SciPost Phys.* **14**, 143 (2023).
- [20] T. Hartweg, T. Gupta, and P. Guido, The bose-hubbard polaron from weak to strong coupling, *arXiv: 2508.00486* (2025).
- [21] N. V. Prokof'ev, B. V. Svistunov, and I. S. Tupitsyn, Worm algorithm in quantum monte carlo simulations, *JETP* **87**, 310 (1998).
- [22] N. V. Prokof'ev, B. V. Svistunov, and I. S. Tupitsyn, “worm” algorithm in quantum monte carlo simulations, *Physics Letters A* **238**, 253 (1998).
- [23] B. Capogrosso-Sansone, G. Söyler, N. V. Prokof'ev, and B. V. Svistunov, Critical entropies for magnetic ordering in bosonic mixtures on a lattice, *Phys. Rev. A* **81**, 053622 (2010).
- [24] F. Lingua, B. Capogrosso-Sansone, A. Safavi-Naini, A. J. Jahanjiri, and V. Penna, Multiworm algorithm quantum monte carlo, *Physica Scripta* **93**, 105402 (2018).
- [25] E. L. Pollock and D. M. Ceperley, Path-integral computation of superfluid densities, *Phys. Rev. B* **36**, 8343 (1987).
- [26] C. Zhang, Evolution of a single impurity across the superfluid-mott insulator transition in the bose-hubbard model, (2026).